Worst-Case Estimation for Data-Dependent Timing Jitter and Amplitude Noise in High-Speed Differential Link

Wei Yao, Yiyu Shi, *Member, IEEE*, Lei He, *Senior Member, IEEE*, and Sudhakar Pamarti, *Member, IEEE*

***Abstract*—Differential signaling has been widely used in high-speed interconnects. Signal integrity issues, such as inter-symbol interference (ISI) and crosstalk between the differential pair, however, still cause significant timing jitter and amplitude noise and heavily limit the performance of the differential link. The pre-emphasis filter is commonly used to reduce ISI but may potentially change the crosstalk behavior. In this paper, we first propose formula-based jitter and noise models considering the combined effect of ISI, crosstalk, and pre-emphasis filter. With the same set of input patterns, experiment shows our models achieve within 5% difference compared with SPICE simulation. By utilizing these formula-based models, we then develop algorithms to directly find out the input patterns for worst-case jitter and worst-case amplitude noise through pseudo-Boolean optimization (PBO) and mathematical programming. In addition, a heuristic algorithm is proposed to further reduce runtime. Experiments show our algorithms obtain more reliable worst-case jitter and noise compared with pseudo-random bit sequences simulation and, meanwhile, reduce runtime by 25× when using a general PBO solver and by 150× when using our proposed heuristic algorithm.**

***Index Terms*—Jitter, modeling, noise, transmission line.**

I. Introduction

DIFFERENTIAL signaling has been widely used in high-speed I/O interconnect standards like PCI-Express and Serial ATA. It has several advantages, such as a high transmission rate due to low signal swing, little electromagnetic interference (EMI), and common-mode noise immunity. Considerable signal integrity issues, however, still limit the link performance and become bottlenecks during system integration. Such issues include resistive losses, reflections, inductive ringing and crosstalk between differential pairs [2], [3].

To evaluate the combined effect of these impairments on the overall system performance, the associated eye diagram [4], [5] has been used as an effective measure. As shown in Fig. 1, the eye diagram is defined as the synchronized superposition of all possible realizations of the signal viewed within a particular signal interval. It provides a fast evaluation of system performance. The width of the eye opening defines the time interval over which the received signal can be sampled without error. The height of the eye opening with the amount of amplitude noise at a specified sampling time defines the signal-to-noise-ratio (SNR) of the received signal [4].

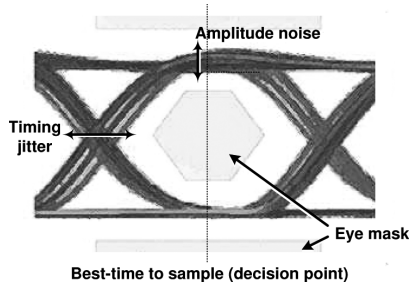

Fig. 1. Eye diagram and eye mask.

Consider the eye diagram shown in Fig. 1. The amounts of timing jitter and amplitude noise determine the width and height of the eye. Jitter is defined as the deviation of the zero-crossing from its ideal occurrence time and decreases the eye's width [6]. Amplitude noise, on the other hand, decreases the SNR and, accordingly, the eye's height. As a result, to determine the performance of the interconnect, we need to consider both timing jitter and amplitude noise simultaneously.

Specifically, inter-symbol interference (ISI) and crosstalk are two major factors that induce jitter and amplitude noise. ISI is defined as one symbol interfering with subsequent symbols and is caused by channel impairments such as attenuation, reflection, and group delay distortion. Crosstalk, on the other hand, is caused by electromagnetic coupling between transmission lines. To counteract ISI, a finite impulse response (FIR) pre-emphasis filter at the transmitter side is widely used to emphasize the signal prior to the impact of the channel [7]–[9]. Pre-emphasized signal, on the other hand, also affects coupled electromagnetic energy and changes crosstalk behavior. As a result, for both ISI and crosstalk, it is important to take pre-emphasis filter into consideration.

Traditionally, the eye diagram is obtained through lengthy time-domain simulation with pseudorandom bit sequences as the input data. In the literature, several types of techniques were proposed to model the eye diagram and tried to efficiently predict the jitter and amplitude noise at the design phase [10]–[15]. However, [10] considers reflection and attenuation with only one input pattern, and [11] only considers a lossless transmission line. As a result, those models are far from accurate. [12], [13] and [14] have a better model because they consider lossy

Manuscript received June 25, 2009; revised March 08, 2010; accepted October 06, 2010. This paper was supported in part by a University of California MICRO grant sponsored by Actel and Fujitsu. An earlier version of this paper was presented at the International Symposium on Quality Electronic Design, San Jose, CA, March 16–19, 2009.

W. Yao, L. He, and S. Pamarti are with the Department of Electrical Engineering, University of California, Los Angeles, CA 90095 USA (e-mail: weiyao@ee.ucla.edu; lhe@ee.ucla.edu; spamarti@ee.ucla.edu).

Y. Shi is with the Electrical and Computer Engineering Department, Missouri University of Science and Technology, Rolla, MO 65409 USA (e-mail: yshi@mst.edu).

Digital Object Identifier 10.1109/TVLSI.2010.2090544

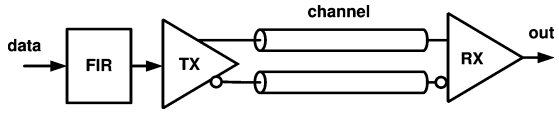

Fig. 2. Transceiver block diagram for differential signaling.

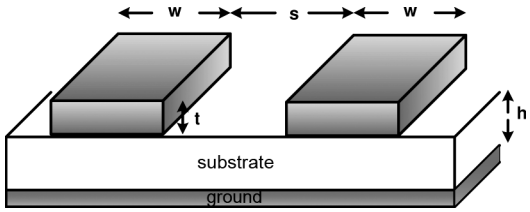

Fig. 3. Section of differential microstrip line.

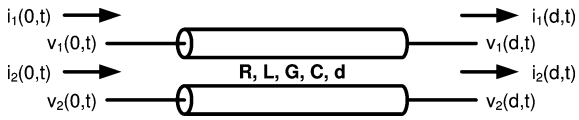

Fig. 4. Parallel transmission lines.

transmission lines, but they still take only a few input patterns into account and use an inaccurate linear approximation. To efficiently handle the input patterns in adequate length, [15] uses the pull-up and pull-down transitions of the signal step response to predict the worst-case eye diagram. This waveform-based method, however, is very sensitive to the transmission environment and only applies to single transmission line without any crosstalk noise. Most importantly, all existing works fail to consider the effect of the pre-emphasis filter, which effectively reduces ISI, as shown in Fig. 6 in Section II, but at the same time affects crosstalk.

In this paper, we first propose formula-based jitter and amplitude noise models that consider the combined effect of ISI, crosstalk, and the pre-emphasis filter for differential signaling. With the same set of input patterns, experiment shows our models achieve within 5% difference compared to SPICE simulation. Note that we apply a RLGC lossy transmission-line model according to differential microstrip-line geometry, and we represent the channel impairments and crosstalk through transmission-line time-domain response. By using these formula-based models, we then develop algorithms to directly predict the input patterns that cause worst-case jitter and worst-case amplitude noise through pseudo-Boolean optimization (PBO) and mathematically programming. Moreover, heuristic algorithm is proposed to further reduce runtime. Experiments show our algorithms obtain more reliable worst-case jitter and noise compared with pseudorandom bit sequences simulation and, meanwhile, reduce runtime by $25\times$ when using general PBO solver and by $150\times$ when using our proposed heuristic algorithm.

The remainder of this paper is organized as follows. Section II reviews background on transmission lines and the pre-emphasis filter. Section III presents our formula-based jitter and noise models. Sections IV and V introduce our problem formulation and algorithms to directly find out input patterns that cause worst-case jitter and amplitude noise. Section VI describes experiments on different transmission lines, and Section VII concludes the paper.

II. Preliminaries

We first review the RLGC model for parallel transmission lines and the frequency-domain relationships between input and output ports. Next, an overview of the transmitter pre-emphasis filter is provided, and its impact on eye diagram is also demonstrated.

A. RLGC Model for Transmission Line

A cross section of the differential microstrip line is shown in Fig. 3. We assume the lines are homogeneous, uniform, and parallel to each other without any variation [11]. The dielectric is assumed to be homogeneous with constant permittivity ε and permeability μ.

The distributed self and mutual inductances are computed with the method of images [16]: the effect of the ground plane is replaced with the image currents. The rectangular shapes of conductors were changed into circular ones for geometry simplification and the following expressions were found for the per-unit-length self and mutual inductances [16]:

$$l = \frac{\mu}{2\pi} ln\left(1 + \frac{2H_{\rm eq}}{r_{\rm eq}}\right) \tag{1}$$

$$m = \frac{\mu}{4\pi} ln\left(\frac{(s_{\rm eq}+2r_{\rm eq})^2 + (r_{\rm eq}+2H_{\rm eq})^2}{(s_{\rm eq}+2r_{\rm eq})^2 + r_{\rm eq}^2}\right) \tag{2}$$

where $H_{\rm eq}$, $r_{\rm eq}$, and $s_{\rm eq}$ are the equivalent height, thickness, and spacing of the differential microstrip line. l is self inductance and m is mutual inductance. The distributed capacitances may be calculated as follows [17]:

$$c_p = \frac{\mu\epsilon m}{l^2 + m^2} \tag{3}$$

$$c = \frac{\mu\epsilon l}{l^2 + m^2}, \tag{4}$$

where c is the distributed capacitance between the conductor and the ground and c_p is the distributed parasitic capacitance between the conductor lines.

By using these analytical parasitics models, the RLGC per-unit-length model for the differential microstrip lines can be established. Note that other field-solver-based tools can also be used for RLGC extraction, and our jitter and noise modeling and estimation algorithm still apply.

B. Parallel Transmission Lines

High-speed signal propagation on an interconnect can be influenced by several effects, such as delay, attenuation, reflection, slew rate limitation, and crosstalk. All of these effects, which are also known as transmission-line effects [18], can be captured by distributed transmission-line equations with an accurate RLGC per-unit-length model. To analyze the three-wire differential signaling, as shown in Fig. 4, we first consider the general multiconductor transmission line system.

Transmission-line characteristics are in general described by Telegrapher's equations and per-unit-length $\boldsymbol{R}$, $\boldsymbol{L}$, $\boldsymbol{G}$, and $\boldsymbol{C}$ matrices [18], [19]:

$$\frac{\partial}{\partial x}\boldsymbol{v}(x,t) = -\boldsymbol{R}i(x,t) - \boldsymbol{L}\frac{\partial}{\partial x}\boldsymbol{i}(x,t) \tag{5}$$

$$\frac{\partial}{\partial x}\boldsymbol{i}(x,t) = -\boldsymbol{G}\boldsymbol{v}(x,t) - \boldsymbol{C}\frac{\partial}{\partial x}\boldsymbol{v}(x,t) \tag{6}$$

where $\boldsymbol{v}$ and $\boldsymbol{i}$ are voltage and current vectors, and $\boldsymbol{R}$, $\boldsymbol{L}$, $\boldsymbol{G}$, and $\boldsymbol{C}$ are the per-unit-length resistance, inductance, conductance, and capacitance matrix for the transmission line, respectively. Taking the Laplace transform of (5) and (6), we can obtain

$$\frac{\partial}{\partial x}\boldsymbol{V}(x,s) = -\boldsymbol{Z}\boldsymbol{I}(x,s) \tag{7}$$

$$\frac{\partial}{\partial x}\boldsymbol{I}(x,s) = -\boldsymbol{Y}\boldsymbol{V}(x,s) \tag{8}$$

where $\boldsymbol{Z}$ and $\boldsymbol{Y}$ are the impedance and admittance matrices, given by

$$\boldsymbol{Z} = \boldsymbol{R} + s\boldsymbol{L} \quad \boldsymbol{Y} = \boldsymbol{G} + s\boldsymbol{C}. \tag{9}$$

Further derivation could be achieved through multiconductor transmission-line decoupling [17]–[19] for lossy identical transmission lines. First differentiating the partial differential equations given in (7) and (8) with respect to x, we get following two coupled equations:

$$\frac{\partial^2}{\partial x^2}\boldsymbol{V}(x,s) = -\boldsymbol{Z}\boldsymbol{Y}\boldsymbol{V}(x,s) \tag{10}$$

$$\frac{\partial^2}{\partial x^2}\boldsymbol{I}(x,s) = -\boldsymbol{Y}\boldsymbol{Z}\boldsymbol{I}(x,s). \tag{11}$$

Decoupling of (10) and (11) can be achieved by introducing a transformation matrix $\boldsymbol{W}$ relating to actual circuit voltage $\boldsymbol{V}$ and modal voltage $\tilde{\boldsymbol{V}}$ [18] as follows:

$$\boldsymbol{V}(x,s) = \boldsymbol{W}\tilde{\boldsymbol{V}}(x,s). \tag{12}$$

Using (12), we can rewrite (10) as

$$\frac{\partial^2}{\partial x^2}\tilde{\boldsymbol{V}}(x,s) = -(\boldsymbol{W}^{-1}\boldsymbol{Z}\boldsymbol{Y}\boldsymbol{W})\tilde{\boldsymbol{V}}(x,s). \tag{13}$$

To successfully decouple the equations, the matrix product in parentheses in (13) must be a diagonal matrix as

$$\boldsymbol{W}^{-1}\boldsymbol{Z}\boldsymbol{Y}\boldsymbol{W} = \begin{bmatrix} \gamma_1^2 & 0 & 0 \\ 0 & \cdots & 0 \\ 0 & 0 & \gamma_N^2 \end{bmatrix} \tag{14}$$

where the transformation matrix $\boldsymbol{W}$ corresponds to the eigenvectors of product $\boldsymbol{Z}\boldsymbol{Y}$, and the resulting diagonal matrix contains the eigenvalues $(\gamma_1, \ldots, \gamma_N)$ of product $\boldsymbol{Z}\boldsymbol{Y}$. The solution of (13) can then be written as

$$\tilde{\boldsymbol{V}}(x) = [\boldsymbol{E}(x)]C_1 + [\boldsymbol{E}(x)]^{-1}C_2 \tag{15}$$

$$\boldsymbol{V}(x) = \boldsymbol{W}[\boldsymbol{E}(x)]C_1 + \boldsymbol{W}[\boldsymbol{E}(x)]^{-1}C_2 \tag{16}$$

where $\boldsymbol{E}(x) = \mathrm{diag}[e^{-\gamma_1 x}, \ldots, e^{-\gamma_N x}]$ and (C_1, C_2) are constants determined by boundary conditions.

Substituting (16) back into (7), we have

$$\boldsymbol{I}(x) = \boldsymbol{W}_i[\boldsymbol{E}(x)]C_1 + \boldsymbol{W}_i[\boldsymbol{E}(x)]^{-1}C_2 \tag{17}$$

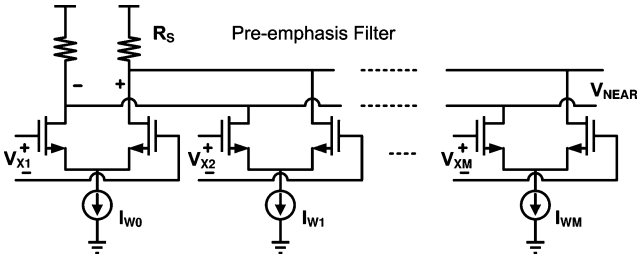

Fig. 5. Pre-emphasis filter at transmitter end for CML differential signaling.

where

$$\boldsymbol{W}_i = Z^{-1}\boldsymbol{W}\boldsymbol{\Gamma} \tag{18}$$

$$\boldsymbol{\Gamma} = \begin{bmatrix} \gamma_1 & 0 & 0 \\ 0 & \cdots & 0 \\ 0 & 0 & \gamma_N \end{bmatrix}. \tag{19}$$

Combining (16) and (17) to eliminate constants (C_1, C_2), the voltage–current relationships between $x = 0$ and $x = d$ in the frequency domain can be expressed as

$$\begin{bmatrix} \boldsymbol{I}(0) \\ -\boldsymbol{I}(d) \end{bmatrix} = \begin{bmatrix} \boldsymbol{Y_{11}} & \boldsymbol{Y_{12}} \\ \boldsymbol{Y_{21}} & \boldsymbol{Y_{22}} \end{bmatrix} \begin{bmatrix} \boldsymbol{V}(\mathbf{0}) \\ \boldsymbol{V}(\boldsymbol{d}) \end{bmatrix} = \begin{bmatrix} \boldsymbol{W_i E_1 W^{-1}} & \boldsymbol{W_i E_2 W^{-1}} \\ \boldsymbol{W_i E_2 W^{-1}} & \boldsymbol{W_i E_1 W^{-1}} \end{bmatrix} \begin{bmatrix} \boldsymbol{V}(\mathbf{0}) \\ \boldsymbol{V}(\boldsymbol{d}) \end{bmatrix} \tag{20}$$

where

$$\boldsymbol{E_1} = \mathrm{diag}\left\{\frac{1 + e^{-2\gamma_k d}}{1 - e^{-2\gamma_k d}}\right\} \tag{21}$$

$$\boldsymbol{E_2} = \mathrm{diag}\left\{\frac{-2e^{-2\gamma_k d}}{1 - e^{-2\gamma_k d}}\right\}, \quad k = 1, 2, \ldots, N \tag{22}$$

where $\boldsymbol{I}(0)$, $\boldsymbol{I}(d)$, $\boldsymbol{V}(0)$, and $\boldsymbol{V}(d)$ are Laplace transforms of $\boldsymbol{i}(0,t)$, $\boldsymbol{i}(d,t)$, $\boldsymbol{v}(0,t)$, and $\boldsymbol{v}(d,t)$, respectively. Here, Y_{11}, Y_{12}, Y_{21}, and Y_{22} form the equivalent admittance matrix or Y-parameters of the transmission line. Please note that the admittance matrix can also be directly obtained from measured response or measured S-parameters.

C. Pre-Emphasis Filter

Using a symbol-spaced FIR filter to pre-emphasize the signal at the transmitter end is a common way to counteract ISI. The filter can be expressed as

$$y(n) = \sum_{i=-N}^{M} W_i x(n-i) \tag{23}$$

where W_i is the coefficient for each filter tap and $x(n)$ and $y(n)$ are the corresponding filter input and output signal. A circuit implementation of the current-mode logic (CML) pre-emphasis driver is shown in Fig. 5. The coefficient of each tap is realized by the current source and requires a dedicated differential pair to drive the output. Normally, the number of taps ranges from two to five because of power and area constraints.

The coefficient of each tap is directly related to the channel characteristic mentioned in the previous subsection and can be determined adaptively by the least-mean-square (LMS) algorithm [7], [8]

$$W_i^{k+1} = W_i^k + \mu\epsilon_k x_{k-i} \tag{24}$$

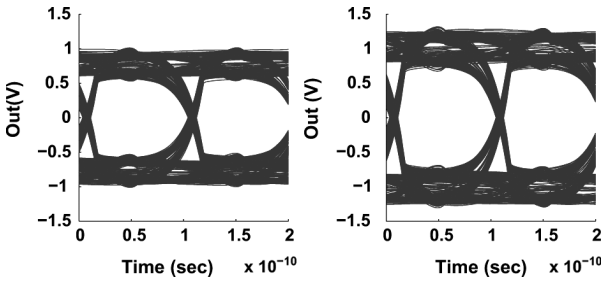

(a) (b)

Fig. 6. Eye diagram (a) without the pre-emphasis filter and (b) with applying a four-tap pre-emphasis filter.

where W is the tap coefficient, μ is the step size, and ϵ_k is the error signal and is defined as the difference between the received signal value and the transmitted value. The convergence of errors drives the coefficients to their optimal value.

To demonstrate the effectiveness of the pre-emphasis filter, the eye diagram with and without the pre-emphasis filter is compared in Fig. 6. The SNR improvement can be clearly seen. As a result, jitter and amplitude noise models cannot capture the actual link performance without considering the existence of a pre-emphasis filter.

III. Jitter and Amplitude Noise Model

The jitter and amplitude noise are actual stochastic processes and can be divided into two categories: random and deterministic. The random part is usually described through a probability density function (PDF) or its root-mean-square (rms) value. On the other hand, the deterministic part is predictable and makes the dominant contribution to the shape of eye diagram [20].

A. Subcomponents of Jitter and Amplitude Noise

Take timing jitter as an example, the total jitter (TJ) is subdivided into two categories: random jitter (RJ) and deterministic jitter (DJ). RJ is a random process and is usually assumed to have a Gaussian distribution because it is mainly contributed by thermal noise [14]. In contrast, DJ is repeatable and predictable. The peak-to-peak value of deterministic jitter is bounded due to its predictable nature. Data-dependent jitter (DDJ), one of the most important sub-component of DJ, is dependent on the bit pattern transmitted on the link under test and is caused by duty-cycle distortion (DCD) and ISI.

Typical crosstalk noise coupling from adjacent data-carrying links belongs to bounded uncorrelated jitter (BUJ). BUJ is bounded due to finite coupling strength, and uncorrelated because there is no correlation to the channel's own data pattern. In this paper, we consider the crosstalk from the adjacent differential link and, as a result, the jitter becomes part of DDJ since we exactly know the transmitted data pattern on the adjacent link.

The PDF of data-dependent jitter and noise are always a series of pulses at the locations where a specific bit pattern experiences a cross over. Therefore, in order to get an accurate measure of the worst case, a large number of bit patterns must be analyzed. As a result, it is critical to find out the worst-case input pattern without doing lengthy simulations. In order to efficiently find out the worst case, we start with formula-based jitter and noise models in the following subsection.

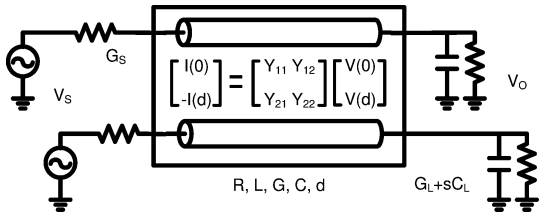

Fig. 7. Differential signaling with parallel transmission lines and termination.

B. Modeling of Data-Dependent Jitter and Noise

To start with, we model the CML transmitter shown in Fig. 5 as an independent voltage source V_s, with matching conductance G_s. At the receiver end, G_L and C_L are used to model the loading conductance and parasitic capacitance of the CML receiver, as shown in Fig. 7. Therefore, the termination constraints become

$$V(0) = V_s - \frac{I(0)}{G_s} \tag{25}$$

$$I(d) = (G_L + sC_L)V(d) \tag{26}$$

and we can derive the frequency domain transfer function using (20), (25), and (26). The result is as follows:

$$V(d) = \tilde{H}V_s(s) = (Y_{12} + (Gs + Y_{11})\tilde{Y})^{-1}Gs \cdot V_s(s) \tag{27}$$

where

$$\tilde{Y} = Y_{21}^{-1}(-Y_{22} - G_L - sC_L). \tag{28}$$

Note that G_s, G_L, and C_L are all 2×2 diagonal matrices. $\tilde{H}$ describes the complete two-port relationship and includes the effect of signal distortion, dispersion, reflection, and all other channel impairments. The frequency-domain relationship between differential input and differential output now becomes

$$H(s) = [1 \quad -1]\,\tilde{H} \begin{bmatrix} \frac{1}{2} \\ -\frac{1}{2} \end{bmatrix}. \tag{29}$$

In order to find the time-domain response, (29) is approximated into the following pole-residue form:

$$H(s) = c + \sum_{i=1}^{q} \frac{k_i}{s - p_i} \tag{30}$$

by using a least-square-approximation-based method [21], where c is a constant and p_i and k_i are the i_{th} out of q poles and residues of $H(s)$. In this way, the time-domain step response $s(t)$ can be obtained through the inverse Laplace transform of $H(s)/s$, and we obtain

$$s(t) = c \cdot u(t) + \sum_{i=1}^{q} \frac{k_i}{p_i}(e^{p_i t} - 1)u(t) \tag{31}$$

where $u(t)$ is the unit step function.

The received signal $r(t)$ at the far-end of the transmission line now can be expressed as

$$r(t) = \sum_{i=-\infty}^{\infty} b_i p(t - iT) \tag{32}$$

where $p(t) = s(t) - s(t-T)$ is the time-domain response of a nonreturn-to-zero (NRZ) symbol, and b_i is the filter's output, which can be evaluated as

$$b_i = \sum_{j=0}^{m-1} W_j a_{i+j} \tag{33}$$

where W_j is the pre-emphasis filter coefficient, a_i is the input symbol pattern, and m is the number of taps in the filter and is the same as shown in (23). Note here that we assume that the input symbol pattern a_i is uncorrelated with each other. However, any linear data correlation, such as encoded data using block coding, can be taken into consideration, and the same problem formulation can be applied when we combine the correlation with the pre-emphasis filter using one single linear expression similar to (33).

We define the reference time point t_0 as the time when the waveform, without interference from neighboring symbols, crosses a certain threshold V_{th} [12], [13]. In other words, t_0 can be solved with

$$p(t_0) = V_{\rm th}, \qquad 0 \le t_0 < T. \tag{34}$$

Jitter is the deviation from such a time point. For a given input pattern, the jitter can be computed as

$$|t_1 - t_0| \tag{35}$$

where $r(t_1) = V_{\rm th}$. On the other hand, the amplitude noise is defined as the amplitude variation at the optimal sampling time, that is,

$$|r(t_s) - p(t_s)| \tag{36}$$

where

$$t_s = \arg\max_t \{p(t)\}. \tag{37}$$

IV. Worst-Case Timing Jitter

The data-dependent jitter and amplitude noise highly depend on the input pattern. In this paper, we develop algorithms that, by using mathematical programming, can directly find out the input patterns for worst-case jitter and worst-case noise without doing lengthy simulations. To start with, the algorithm for worst-case jitter is proposed in this section.

A. Problem Formulation

The worst jitter is the sum of the maximal positive deviation $t_1 - t_0 (t_1 > t_0)$ and the maximal negative deviation $t_0 - t_1 (t_0 > t_1)$. For simplicity of presentation, we only discuss how to compute the maximal positive deviation. It should be understood that the same procedure can be applied to compute the maximal negative deviation as well. We can formulate the maximal positive deviation as the following integer nonconvex programming problem $(\mathbf{P1})$:

$$(\mathbf{P1}) \quad \max_{a_i} \quad t_1 - t_0 \tag{38}$$

$$\text{subject to} \quad \sum_{i=-\infty}^{\infty} b_i r(t_1 - iT) = V_{\rm th} \tag{39}$$

$$t_0 \le t_1 < T \tag{40}$$

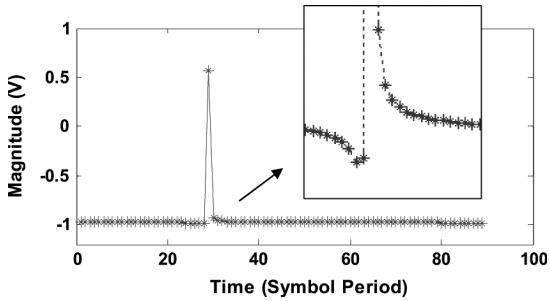

Fig. 8. Time-domain response of the channel.

$$b_i = \sum_{j=0}^{m-1} W_j a_{i+j} \tag{41}$$

$$a_i \in \{0, 1\} \tag{42}$$

where t_0 is defined in (34) given zero-crossing threshold $V_{\rm th}$. $r(t)$ is the time-domain response for one-bit transmission as shown in Fig. 8. a_i and b_i are pre-emphasis filter's input and output with W_j is the filter's coefficient for tap j.

Note that $r(t)$ attenuates quickly as time goes to infinity, as shown in Fig. 8. Thus, (39) can be well approximated by

$$\sum_{i=-N}^{N} b_i r(t_1 - iT) = V_{\rm th} \tag{43}$$

where N can be decided such that the error is within certain bound

$$|b_N r(t - NT)| < |\epsilon r(t)| \qquad \forall\, 0 \le t < T \tag{44}$$

and ϵ is in $[0, 1]$ and is specified by user. A larger ϵ reduces the problem complexity, but introduces more significant error.

B. Relaxation-Based Binary Search

If we assign a set of values to t_1, then the problem becomes a nonlinear feasibility problem and can be solved through an efficient heuristic method, i.e., for each value of t_1, we test whether a combination of the symbols a_i can be found such that (39) holds and then pick the t_1 that maximizes $t_1 - t_0$ among all of the feasible solutions. Such a problem structure enables us to use the binary search technique on t_1, which is bounded in $[t_0, T)$. However, the main difficulty lies in the fact that the feasible space for t_1 is not continuous. If we randomly assign values to t_1, the chance for it to be feasible is slim.

To overcome this difficulty, instead of finding a set of symbols that satisfies (39), we look for a nearby feasible value as an alternative, if possible. This is done by the following procedure. Suppose t_1 is assigned with value $\tilde{t}_1$. Then, the corresponding feasibility problem would be

$$\sum_{j=-N}^{N} b_j r(\tilde{t}_1 - jT) =, V_{\rm th} \tag{45}$$

$$0 \le \tilde{t}_1 < T \tag{46}$$

$$b_j = \sum_{i=0}^{m-1} W_i a_{i+j}, \qquad -N \le j \le N \tag{47}$$

$$a_j \in \{0, 1\}, \qquad -N \le j \le N + m - 1. \tag{48}$$

C. PBO

We first show how to reformulate the problem so that we can use a general pseudo-Boolean solver as the core of our binary search algorithm.

Once t_1 is assigned with value $\tilde{t}_1$ within the binary search, the value of $r(\tilde{t}_1 - jT)$ in (45) can be calculated easily and become a known variable to us, denoted as r_j. Along with (47), as a result, the constraints in the original feasibility problem now become

$$\sum_{j=-N}^{N+m-1} c_j a_j = d \tag{49}$$

$$a_j \in \{0,1\}, \qquad -N \le j \le N+m-1 \tag{50}$$

where $c_j = \sum_{k=-N}^{j} r_k W_{j-k}$ and $d = V_{\text{th}}$ are some constants that can be derived from (45) and (47), given the value of $\tilde{t}_1$. The resulted problem becomes that can we find at least one feasible solution, which each a_j is restricted to either 0 or 1, satisfies a linear equality constraint.

To solve this problem, we can simply relax the equality constraint by adding an error term ϵ and convert the equality constraint into two inequality constraints, as shown in problem (P2): $(\mathbf{P2})$

$$(\mathbf{P2}) \quad \min \quad t \tag{51}$$

$$\text{subjectto} \quad \sum_{j=-N}^{N} c_j a_j \le d + \epsilon t \tag{52}$$

$$\sum_{j=-N}^{N} (-c_j) a_j \le -d + \epsilon t \tag{53}$$

$$a_j \in \{0,1\}, \qquad t \in \{0,1\} \tag{54}$$

$$-N \le j \le N+m-1. \tag{55}$$

Note that an extra variable t is added to convert the feasibility problem into an optimization problem.

(P2) is actually an instance of the pseudo-Boolean optimization (PBO) problem, which generally has the following structure:

$$\min \quad \sum_{j=1}^{n} c_j \cdot x_j \tag{56}$$

$$\text{s.t.} \quad \sum_{j=1}^{n} b_{ij} l_j \le d_i \tag{57}$$

$$x_j \in \{0,1\}, \qquad i \in \{1 \ldots m\} \tag{58}$$

where x_j is a Boolean variable and a literal l_j denotes either a variable x_j or its complement $\bar{x}_j$. The PBO can be solved by using existing pseudo-Boolean solver. In this paper, we use miniSAT+ [22], a SAT-based pseudo-Boolean solver, to solve (P2) in our experiment, given the error bound defined by ϵ. Note that, if a given t_1 value is feasible with error bound ϵ, the SAT-based pseudo-Boolean solver returns a feasible input pattern $\tilde{a}_j$. Then, we can use the pattern to calculate the timing jitter t_1 using (43) and use it as the new bound in the binary search algorithm.

Note that due to the complexity of our original problem, there is neither guarantee for optimal solution nor meaningful upper bound of runtime complexity for the combined relaxation-based binary search and pseudo-Boolean optimization. Experimental results, however, show that our algorithm gives more pessimistic result than brute-force enumeration method, yet achieve significant runtime reduction. In the following section, we further propose a heuristic algorithm replacing PBO solver to reduce runtime.

D. Proposed Heuristic

Instead of solving the feasibility problem through pseudo-Boolean solver, in this paper, we propose a heuristic algorithm based on the specific structure of our problem so that we can solve it more efficiently.

To begin with, we first relax the integer constraint (48) to

$$0 \le a_j \le 1, \qquad -N \le j \le N+m-1 \tag{59}$$

and solve the problem $(\mathbf{P3})$

$$(\mathbf{P3}) \quad \max \quad \sum_{j=-N}^{N+m-1} |a_j - 0.5| \tag{60}$$

$$\text{s.t.} \quad b_j = \sum_{i=0}^{m-1} W_i a_{i+j}, \qquad -N \le j \le N \tag{61}$$

$$\sum_{j=-N}^{N} b_j r(\tilde{t}_1 - jT) = V_{\text{th}} \tag{62}$$

$$0 \le a_j \le 1, \qquad -N \le j \le N+m-1. \tag{63}$$

The objective function (60) tries to find the solution set a_j that is as close to the integer as possible. For the time being, let us assume that we know how to solve $(\mathbf{P3})$. Then, we denote the optimal solution as $\tilde{a}_j$ and round it to 0 or 1. After that, we can get $\tilde{b}_j$ from (61), and insert them in the equation

$$\sum_{j=-N}^{N} \tilde{b}_j r(t_1 - jT) = V_{\text{th}} \tag{64}$$

to solve for t_1, which is close to $\tilde{t}_1$ and yet is a feasible solution of the original problem. This procedure can now be used as the core for the binary search. The overall algorithm for jitter computation is shown in Algorithm 1, where ϵ_0 is used to control the termination condition: when the lower bound and upper bound have a difference smaller than ϵ_0, the search stops.

Now we discuss how problem $(\mathbf{P3})$ can be solved efficiently. For the sake of efficiency, we propose an heuristic to obtain its solution directly from the structure of $(\mathbf{P3})$. Let

$$x_j = a_j - 0.5, \qquad -N \le j \le N+m-1 \tag{65}$$

and insert (61) into (62). Then, $(\mathbf{P3})$ can be transformed into an equivalent form

$$\max \quad \sum_{j=-N}^{N+m-1} |x_j| \tag{66}$$

$$\text{s.t.} \quad \sum_{j=-N}^{N+m-1} c_j x_j = d \tag{67}$$

$$-0.5 \le x_j \le 0.5, \qquad -N \le j \le N+m-1 \tag{68}$$

where c_j and d are some constants that can be derived easily.

TABLE I
DIFFERENTIAL TRANSMISSION-LINE TESTBENCH DESIGN INFORMATION: WIDTH(W), SPACING(S), THICKNESS(T), DIELECTRIC HEIGHT(H), LENGTH(L), AND CHARACTERISTIC IMPEDANCE

Design	w (um)	s (um)	t (um)	h (um)	L (cm)	Char. impedance
#1	100	193.86	10	300	15	49.03
#2	50	117.48	50	200	15	49.2
#3	50	117.48	50	200	25	49.2
#4	100	80	10	300	15	52.51
#5	50	500	10	300	30	58.55

The incentive of the heuristic to be proposed below is to let as many x_i take the maximum absolute value as possible. Due to the symmetry of the problem, without loss of generosity, we can assume

$$|c_{-N}| \leq |c_{-N+1}| \cdots \leq |c_k| \leq |c_{k+1}| \leq |c_{N+m-1}|. \quad (69)$$

Then, according to this ascending order of $|c_i|$, we assign -0.5 or 0.5 as the optimal value $\tilde{x}_i$ based on the following criteria:

$$\tilde{x}_i = \begin{cases} -sgn(c_i) \times 0.5, & \text{if } d - \sum_{j=-N}^{i-1} c_j x_j > 0 \\ sgn(c_i) \times 0.5, & \text{otherwise.} \end{cases} \quad (70)$$

This assignment is continued until

$$\sum_{j=i+1}^{N+m-1} 0.5|c_j| < d - \sum_{j=-N}^{i} c_j \tilde{x}_j \quad (71)$$

and the solutions for the remaining x_i are

$$\tilde{x}_i = sgn(c_i) \times \frac{\sum_{j=-N}^{i} c_j \tilde{x}_j - d}{|c_i|}. \quad (72)$$

Again, due to the complexity of the original problem, we cannot guarantee that the solution obtained from our algorithm is optimal (or even locally optimal). However, experimental results show that our algorithm gives a result that is very close or more pessimistic to the enumeration method, yet achieves further speedup compared with using a PBO solver. The overall algorithm for solving problem $(\mathbf{P1})$ is summarized in Algorithm 1.

Algorithm 1 Algorithm for solving problem $(\mathbf{P1})$

Initialize:$t_1^{lb} = t_0$;$t_1^{ub} = T$;
while $t_1^{lb} < t_1^{ub} - \epsilon_0$ **do**
$\tilde{t}_1 = (t_1^{lb} + t_1^{ub})/2$;
Solve problem $(\mathbf{P3})$ for $\tilde{a}_i$ and round it to 0 or 1.
Compute $\tilde{b}_i$ based on the rounded $\tilde{a}_i$ from **(61)**;
Solve **(64)** for t_1;
if $t_1 > t_1^{lb}$ **then**
$t_1^{lb} = t_1$;
else
$t_1^{ub} = \tilde{t}_1$;
end if
end while
Return t_1^{lb};

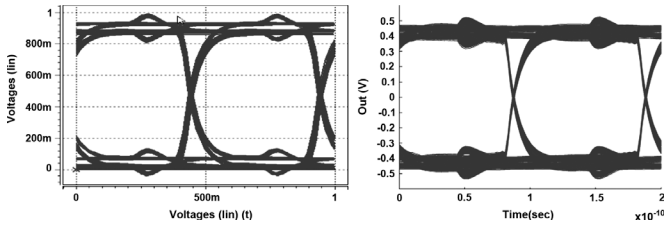

(a) (b)

Fig. 9. Transient simulation comparison between (a) SPICE and (b) our model. The origin point is different.

TABLE II
JITTER AND AMPLITUDE NOISE MODEL VALIDATION

	SPICE			Our Model		
	Jitter (ps)	Noise (V)	Runtime (sec)	Jitter (ps)	Noise (V)	Runtime (sec)
#1	11.8	0.27	0.26	11.9	0.27	0.17
#2	5.0	0.20	0.26	5.0	0.21	0.17
#3	4.6	0.20	0.25	4.7	0.19	0.16
#4	11.0	0.29	0.26	10.5	0.30	0.17
#5	7.7	0.11	0.23	7.7	0.11	0.18
Avg. relative error				1.1%	2.8%	

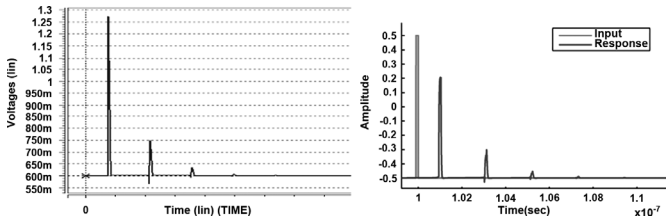

(a) (b)

Fig. 10. Time-domain response. (a) SPICE simulation. (b) MATLAB simulation with our model. The origin point is different.

V. WORST-CASE AMPLITUDE NOISE

The amplitude noise is the difference between the maximum amplitude deviation and the minimum amplitude deviation, at the optimal sampling time. To find the worst-case noise, we could use the following formulation:

$$(\mathbf{P4}) \quad \max_{a_i} \text{ or } \min_{a_i} \quad \sum_{i=-N}^{N} b_i r(t_s - iT) \quad (73)$$

$$\text{s.t.} \quad b_i = \sum_{j=0}^{m-1} W_j a_{i+j} \quad (74)$$

$$a_i \in \{0, 1\} \quad (75)$$

where

$$t_s = \arg\max_t \{p(t)\} \quad (76)$$

is the optimal sampling time. The difference between maximum and minimum deviation determines the peak-to-peak amplitude noise for the eye diagram. Given the t_s calculated from (76), we can rewrite $(\mathbf{P4})$ as (use the maximum problem as an example)

$$\max_{a_i} \quad \sum_{i=-N}^{N+m-1} c_i a_i \quad (77)$$

TABLE III
WORST-CASE JITTER, AMPLITUDE NOISE AND RUNTIME COMPARISON. PRBS: DENOTES PSEUDORANDOM BIT SEQUENCE. FOR WORST-CASE JITTER; RELAXATION-BASED BINARY SEARCH (BS) IS USED ALONG WITH PBO OR OUR HEURISTIC ALGORITHM (HEURISTIC). FOR WORST-CASE NOISE, LP DENOTES DIRECTLY SOLVING LINEAR PROGRAMMING

	Worst-case Jitter (ps)			Worst-case Noise (volts)		Total runtime (sec)		
	PRBS	BS+PBO	BS+Heuristic	PRBS	LP	PRBS	BS+PBO+LP	BS+Heuristic+LP
#1	16	15	16	0.34	0.36	37.8	1.56	0.25
#2	8	8	8	0.25	0.27	38.9	1.55	0.25
#3	9	10	9	0.25	0.30	38.2	1.56	0.26
#4	20	25	24	0.37	0.41	37.8	1.50	0.26
#5	12	12	12	0.14	0.17	37.9	1.55	0.26

$$\text{s.t.} \quad a_i \in \{0,1\} \tag{78}$$

where $c_i = \sum_{k=-N}^{i} r_k W_{i-k}$ and $r_k = r(t_s - kT)$ can be derived from (73) and (74). As a result, it is a linear programming problem and, moreover, the solution can be obtained directly without calling the general linear programming solver. Obviously, to maximize the objective function, we just let a_i be 1 if c_i is positive and be 0 if c_i is negative [23]. For the minimum case, it is vice versa. So the amplitude noise can be expressed as

$$\sum_{i=-N}^{N+m-1} |c_i| \tag{79}$$

and the complexity is $O(N^2)$ given $m \ll N$.

VI. EXPERIMENTAL RESULTS

Here, we report our experiments on a Pentium 4 computer with 2.66-G CPU and 1-G RAM.

A. Jitter and Amplitude Noise Model Validation

We first verify our transmission-line channel model. Table I lists the detailed design information for our various testbench. Fig. 9 shows the comparison of the transient simulation result between our analytical channel model and SPICE simulation for Design 1, given the same RLGC model for channel and the same pre-emphasis filter coefficients. The RLGC value for the channel can be calculated by giving the geometry parameters and using the methods as discussed in Section II-A. For example, the resulted RLGC values for Design 1 are $r = 17.24\,\Omega$, $l = 325$ nH, $m = 119$ nH, $c = 135$ pF, and $c_p = 49$ pF. From Fig. 9, we can find out that the transient behavior is pretty similar and both give the same amount of timing jitter and amplitude noise. Note that the origin point is different between SPICE and our model. This is due to different input setting and does not affect the noise and jitter measurement.

Next, we verify our jitter and noise model with SPICE given the same set of input patterns in Table II. The test pattern contains 100 symbol with a data rate at 10 Gb/s. From Table II, we discover that, given the same input pattern, our model can accurately calculate jitter and noise with similar runtime, compared to SPICE results. The error is within 4.5% for timing jitter and 5% for amplitude noise. Although the runtime improvement is not much, our model is easier to be embedded into other tools or algorithms.

To emphasize the importance of considering a long period of time-domain response, Fig. 10 shows the time-domain response for Design 5, but with unmatched termination resistance. The impedance mismatch at the receiver end will cause severe signal reflection. From Fig. 10, both SPICE simulation and our model clearly illustrate the signal reflection behavior. As a result, only a few taps of the time-domain response is not sufficient to determine the jitter and noise performance.

B. Worst-Case Jitter and Amplitude Noise Calculation

The worst-case jitter, amplitude noise, and runtime comparison for various design cases are listed in Table III. The pre-emphasis filter is optimized in advance for different channel characteristics. The jitter and amplitude performance is calculated through our formula-based model and we consider 40 taps of transmission line time domain response. We first test 10 000 sets of pseudorandom bit sequences (PRBS) in order to find the worst-case scenario for both jitter and noise. We then use relaxation-based binary search to directly determine the required input pattern for the worst-case jitter and solve the linear programming (LP) problem for the worst-case amplitude noise. Moreover, within the relaxation-based binary search for worst-case jitter, two different methods are compared: PBO using miniSAT+ [22] and our proposed heuristic algorithm. Table III shows that, for all of the cases, our algorithm obtains more reliable worst-case jitter and noise compared with PRBS simulations. For worst-case jitter, the results are similar no matter we use PBO solver or the proposed heuristic algorithm but the heuristic algorithm provides better runtime. From Table III, it shows our algorithm obtains worst-case jitter and noise by up to 20% bigger than PRBS. At the same time, our algorithm is $25\times$ faster than PRBS when we use binary search and PBO solver for worst-case jitter and solve LP for worst-case noise and $150\times$ faster than PRBS when we replace the PBO solver with our proposed heuristic algorithm.

VII. CONCLUSION

This paper develops efficient algorithms to calculate the worst-case data-dependent jitter and noise directly for a differential microstrip line without lengthy simulation. We first propose formula-based jitter and noise models that consider the combined effect of ISI, crosstalk, and the pre-emphasis filter. With the same set of input patterns, our models achieve within 5% difference compared to SPICE simulation. By utilizing these formula-based models, we then use binary search along with PBO and mathematical programming to directly predict the input patterns that cause worst-case jitter and worst-case amplitude noise. Experiments show our algorithms obtain more reliable worst-case jitter and noise compared with PRBS simulation and, meanwhile, achieve a $25\times$ runtime reduction when using binary search and PBO solver for worst-case jitter and solving LP for worst-case noise. In addition, by replacing the PBO solver with our proposed heuristic algorithm, a further $150\times$ runtime reduction compared with PRBS can be achieved. Note that our modeling and algorithms are not restricted to

differential signaling and can be applied to any multiconductor transmission lines.

REFERENCES

[1] W. Yao, Y. Shi, L. He, and S. Pamarti, "Worst case timing jitter and amplitude noise in differential signaling," in *Proc. Int. Symp. Quality Electron. Design (ISQED)*, San Jose, CA, Mar. 16–19, 2009.

[2] V. Stojanovic and M. Horowitz, "Modeling and analysis of high-speed links," in *Proc. IEEE Custom Integr. Circuits Conf.*, Sep. 2003, pp. 589–594.

[3] J. Buckwalter and A. Hajimiri, "Crosstalk-induced jitter equalization," in *Proc. IEEE Custom Integr. Circuits Conf.*, Sep. 2005, pp. 409–412.

[4] S. Haykin, *Communication Systems*. New York: Wiley, 2000.

[5] G. Breed, "Analyzing signals using the eye diagram," *High Frequency Electron.*, pp. 50–53, Nov. 2005.

[6] A. Kuo, R. Rosales, T. Farahmand, S. Tabatabaei, and A. Ivanov, "Crosstalk bounded uncorrelated jitter (buj) for high-speed interconnects," *IEEE Trans. Instrum. Meas.*, vol. 54, no. 4, pp. 1800–1810, Oct. 2005.

[7] M. Li, S. Wang, Y. Tao, and T. Kwasniewski, "Fir filter optimisation as pre-emphasis of high-speed backplane data transmission," *Electron. Lett.*, vol. 40, pp. 912–913, Jul. 2004.

[8] Y. Tao, W. Bereza, R. Patel, S. Shumarayev, and T. Kwasniewski, "A signal integrity-based link performance simulation platform," in *Proc. IEEE Custom Integr. Circuits Conf.*, Sep. 2005, pp. 725–728.

[9] J. Kim, J. Lee, E. Song, J. Jo, and J. Kim, "Compensation of undesired channel effects by frequency domain optimization of pre-emphasis filter for over gbps signaling," in *Proc. IEEE Int. Symp. Electromagn. Compatibil.*, Aug. 2006, vol. 3, pp. 721–726.

[10] M. Hashimoto, J. Siriporn, A. Tsuchiya, H. Zhu, and C.-K. Cheng, "Analytical eye-diagram model for on-chip distortionless transmission lines and its application to design space exploration," in *Proc. IEEE Custom Integr. Circuits Conf.*, Sep. 2007, pp. 869–872.

[11] V. Popescu, B. Kirei, M. Topa, and C. Munteanu, "Analysis of lossless differential microstrip line," *Proc. 30th Int. Electron. Technol. Spring Seminar*, pp. 551–554, May 2007.

[12] J. Buckwalter, B. Analui, and A. Hajimiri, "Data-dependent jitter and crosstalk-induced bounded uncorrelated jitter in copper interconnects," in *IEEE MTT-S Int. Microw. Symp. Dig.*, Jun. 2004, vol. 3, pp. 1627–1630.

[13] J. Buckwalter and B. Analui, "Predicting data-dependent jitter," *IEEE Trans. Circuits Syst. II, Exp. Briefs*, vol. 51, no. 9, pp. 453–457, Sep. 2004.

[14] N. Ou, T. Farahmand, A. Kuo, S. Tabatabaei, and A. Ivanov, "Jitter models for the design and test of gbps-speed serial interconnects," *IEEE Design Test Comput.*, vol. 21, pp. 302–313, Jul.-Aug. 2004.

[15] R. Shi, W. Yu, Y. Zhu, C.-K. Cheng, and E. Kuh, "Efficient and accurate eye diagram prediction for high speed signaling," in *Proc. IEEE/ACM Int. Conf. Comput.-Aided Des.*, Nov. 2008, pp. 655–661.

[16] H. Ymeri, B. Nauwelaers, K. Maex, and D. D. Roest, "Broadband impedance parameters of symmetric coupled coplanar CMOS interconnects," *Electrotechn. Rev.*, 2003.

[17] C. R. Paul, *Introduction to Electromagnetic Compatibility*, 2nd ed. New York: Wiley Interscience, 2006.

[18] R. Achar and M. Nakhla, "Simulation of high-speed interconnects," *Proceedings of the IEEE*, vol. 89, pp. 693–728, May 2001.

[19] T. Tang and M. Nakhla, "Analysis of high-speed vlsi interconnects using the asymptotic waveform evaluation technique," *IEEE Trans. Comput.-Aided Des. Integr. (CAD) Circuits Syst.*, vol. 11, no. 3, pp. 341–352, Mar. 1992.

[20] K. K. Kim, J. Huang, Y.-B. Kim, and F. Lombardi, "On the modeling and analysis of jitter in ate using matlab," in *Proc. 20th IEEE Int. Symp. Defect and Fault Tolerance in VLSI Syst.*, Oct. 2005, pp. 285–293.

[21] W. Beyene and J. Schutt-Aine, "Efficient transient simulation of high-speed interconnects characterized by sampled data," *IEEE Trans. Compon., Packaging, Manuf. Technol., B, Adv. Packaging*, vol. 21, no. , pp. 105–114, Feb. 1998.

[22] N. Een and N. Sorensson, "Translating pseudo-Boolean constraints into sat," *JSAT*, vol. 2, pp. 1–26, 2006.

[23] P. Hanumolu, G.-Y. Wei, and U.-K. Moon, "Equalizers for high-speed serial links," *Int. J. High Speed Electron. Syst.*, vol. 15, no. 2, pp. 429–458, 2005.

Wei Yao received the B.S. degree in electrical engineering and M.S. degree in electronics engineering from National Taiwan University, Taipei, Taiwan, in 2002 and 2004, respectively. He is currently working toward the Ph.D. degree in electrical engineering at the University of California, Los Angeles.

From 2004 to 2006, he was a Software Engineer with Synopsys Taiwan, Taipei, Taiwan, working on VLSI power integrity. In 2010, he was with the ASIC Service Department, Taiwan Semiconductor Manufacturing Company, Hsinchu, Taiwan, developing tape-out design flow on signal and power integrity. His current research interests include power integrity, signal integrity, and high-speed mixed-signal circuits.

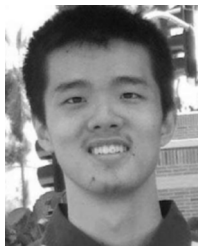

Yiyu Shi (M'10) received the B.S. degree (with honors) in electronic engineering from Tsinghua University, Beijing, China, in 2005, and the M.S. and Ph.D. degree in electrical engineering from the University of California, Los Angeles, in 2007 and 2009, respectively.

He is currently an Assistant Professor with the Electrical and Computer Engineering Department, Missouri University of Science and Technology, Rolla. His current research interests include advanced design and test technologies for 3-D ICs and renewable energy applications.

Dr. Shi was the recipient of the IBM Invention Achievement Award in 2009 and five nominations for the Best Paper Award at various conferences.

Lei He (SM'10) received the Ph.D. degree in computer science from the University of California, Los Angeles (UCLA), in 1999.

He is a Professor with the Electrical Engineering Department, University of California, Los Angeles (UCLA), and was a faculty member with the University of Wisconsin, Madison, between 1999 and 2002. He also held visiting or consulting positions with Cadence, Empyrean Soft, Hewlett-Package, Intel, and Synopsys and was a Technical Advisory Board Member for Apache Design Solutions and Rio Design Automation. He has published one book and over 200 technical papers. His research interests include modeling and simulation, VLSI circuits and systems, and cyber physical systems.

Dr. He was the recipient of 12 Best Paper nominations mainly from the Design Automation Conference and the International Conference on Computer-Aided Design and five Best Paper or Best Contribution Awards, including the 2010 ACM Transactions on Electronic System Design Automation Best Paper Award.

Sudhakar Pamarti (M'03) received the B.Tech. degree in electronics and electrical communication engineering from the Indian Institute of Technology, Kharagpur, India, in 1995, and the M.S. and Ph.D. degrees in electrical engineering from the University of California, San Diego, in 1999 and 2003, respectively.

Since 2005, he has been an Assistant Professor of electrical engineering with the University of California, Los Angeles (UCLA), where he teaches and conducts research in the design of mixed-signal circuits for wireless and wire-line communication systems. Prior to joining UCLA, he worked with Rambus Inc. (2003–2005) designing high-speed chip-to-chip electrical interfaces and with Hughes Software Systems (1995–1997) developing real-time, embedded software for a wireless communication system. His current research interests include mixed-signal circuits, signal processing, and digital communications.

Dr. Pamarti was a recipient of the National Science Foundation CAREER Award.